Demonstration of enhanced K-edge angiography utilizing a samarium x-ray generator

Eiichi Sato*[a], Etsuro Tanaka[b], Hidezo Mori[c], Toshiaki Kawai[d], Takashi Inoue[e], Akira Ogawa[e], Mitsuru Izumisawa[f], Kiyomi Takahashi[g], Shigehiro Sato[g], Toshio Ichimaru[h] and Kazuyoshi Takayama[i]

[a]Department of Physics, Iwate Medical University, 3-16-1 Honchodori, Morioka 020-0015, Japan
[b]Department of Nutritional Science, Faculty of Applied Bio-science, Tokyo University of Agriculture, 1-1-1 Sakuragaoka, Setagaya-ku 156-8502, Japan
[c]Department of Cardiac Physiology, National Cardiovascular Center Research Institute, 5-7-1 Fujishirodai, Suita, Osaka 565-8565 Japan
[d]Electron Tube Division #2, Hamamatsu Photonics K.K., 314-5 Shimokanzo, Iwata 438-0193, Japan
[e]Department of Neurosurgery, School of Medicine, Iwate Medical University, 19-1 Uchimaru, Morioka 020-8505, Japan
[f]Department of Oral Radiology, School of Dentistry, Iwate Medical University, 1-3-27 Chuo, Morioka 020-0021, Japan
[g]Department of Microbiology, School of Medicine, Iwate Medical University, 19-1 Uchimaru, Morioka 020-8505, Japan
[h]Department of Radiological Technology, School of Health Sciences, Hirosaki University, 66-1 Honcho, Hirosaki 036-8564, Japan
[i]Tohoku University Biomedical Engineering Research Organization, 2-1-1 Katahira, Sendai 980-8577, Japan

ABSTRACT

The samarium-target x-ray tube is useful in order to perform cone-beam K-edge angiography because K-series characteristic x-rays from the samarium target are absorbed effectively by iodine-based contrast media. This generator consists of the following components: a constant high-voltage power supply, a filament power supply, a turbomolecular pump, and an x-ray tube. The x-ray tube is a demountable diode which is connected to the turbomolecular pump and consists of the following major devices: a samarium target, a tungsten hairpin cathode (filament), a focusing (Wehnelt) electrode, a polyethylene terephthalate x-ray window 0.25 mm in thickness, and a stainless-steel tube body. In the x-ray tube, the positive high voltage is applied to the anode (target) electrode, and the cathode is connected to the tube body (ground potential). In this experiment, the tube voltage applied was from 50 to 70 kV, and the tube current was regulated to within 0.10 mA by the filament temperature. The exposure time is controlled in order to obtain optimum x-ray intensity. The electron beams from the cathode are converged to the target by the focusing electrode, and bremsstrahlung x-rays were absorbed using a 50-μm-thick tungsten filter. The x-ray intensity was 1.04 μGy/s at 1.0 m from the x-ray source with a tube voltage of 60 kV and a tube current of 0.10 mA, and angiography was performed using a computed radiography system and iodine-based microspheres 15 μm in diameter. In angiography of non-living animals, we observed fine blood vessels of approximately 100 μm with high contrasts.

Keywords: K-series characteristic x-rays, samarium target, demountable x-ray tube, enhanced K-edge angiography

1. INTRODUCTION

Hard X-Ray and Gamma-Ray Detector Physics and Penetrating Radiation Systems VIII, edited by Larry A. Franks, Arnold Burger, Ralph B. James, H. Bradford Barber, F. Patrick Doty, Hans Roehrig, Proc. of SPIE Vol. 6319, 63190L, (2006) · 0277-786X/06/$15 · doi: 10.1117/12.679234

Recent advances in x-ray technology aim at forming monochromatic parallel x-ray beams using synchrotrons in conjunction with silicon crystals. These beams have been applied in preliminary experiments for medical radiography including enhanced K-edge angiography[1,2] using iodine media. In angiography, monochromatic x-rays with photon energies ranging from 33.3 to 35 keV have been employed because the rays are absorbed effectively by iodine-based contrast media with an iodine K-edge of 33.2 keV.

From weakly ionized linear plasmas[3-6] of nickel and copper, extremely clean characteristic x-rays have been produced. In particular, we confirmed the irradiation of the second and fourth harmonic x-rays of the fundamental K-series characteristic x-rays from a copper target. The x-ray intensities of the harmonics increased with increases in the charging voltage, and the harmonic bremsstrahlung rays survived due to the x-ray resonation in the plasma.

Steady-state monochromatic x-ray generators[7] have been developed to produce clean K-series characteristic x-rays utilizing the angle dependence of bremsstrahlung x-rays, since bremsstrahlung rays are not emitted in the opposite direction to that of electron trajectory. Subsequently, a cerium x-ray generator[8-10] has been developed, and has been employed to perform enhanced K-edge angiography achieved with cerium $K\alpha$ rays and iodine-based contrast media, since $K\alpha$ rays (34.6 keV) are absorbed effectively by iodine. In this case, because the sampling pitch of a computed radiography system[11] (Konica Minolta Regius 150) is 87.5 μm, the spatial resolution of approximately 100 μm has been obtained.

To increase the K-series characteristic x-ray intensity, the tube current should be maximized at a constant tube voltage. Therefore, the melting temperature of the target element should be increased because the temperature of the cerium is 1072 K. In view of this situation, a samarium target can be employed, since the $K\alpha$ rays (39.9 keV) from a samarium target are also absorbed effectively by iodine, and the melting temperature is 1350 K.

In the present research, we developed a new samarium x-ray generator and performed a preliminary study on enhanced K-edge angiography achieved with samarium K-series characteristic x-rays.

2. GENERATOR

Figure 1 shows a block diagram of a compact characteristic (quasi-monochromatic) x-ray generator. This generator consists of the following components: a constant high-voltage power supply (SL150, Spellman), a DC filament power supply, a turbomolecular pump, and an x-ray tube. The x-ray tube is a demountable diode which is connected to the turbomolecular pump with a pressure of approximately 0.5 mPa and consists of the following major devices: a samarium rod target of 6.5 mm in diameter, a tungsten hairpin cathode (filament), a focusing (Wehnelt) electrode, a polyethylene terephthalate x-ray window 0.25 mm in thickness, and a stainless-steel tube body (Fig. 2). In the x-ray tube, the positive high voltage is applied to the anode (target) electrode, and the cathode is connected to the tube body (ground potential). In this experiment, the tube voltage applied was from 50 to 70 kV, and the tube current was regulated to within 0.10 mA by the filament temperature. The exposure time is controlled in order to obtain optimum x-ray intensity. The electron beams from the cathode are converged to the target by the focusing electrode, and x-rays are produced through the focusing electrode.

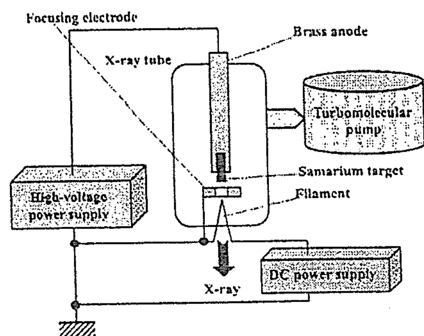

Fig. 1. Block diagram of the x-ray generator with a samarium-target radiation tube, which is used specially for K-edge angiography using iodine-based contrast media.

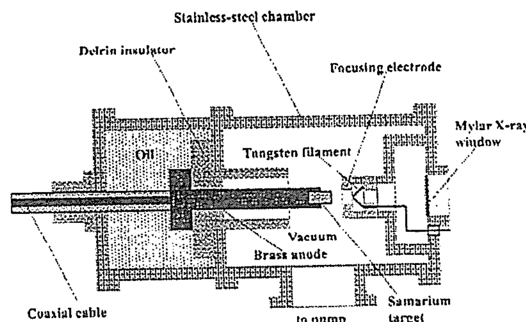

Fig. 2. Structure of the x-ray tube with a samarium target

3. CHARACTERISTICS

3.1 X-ray intensity

The x-ray intensity was measured by a Victoreen 660 ionization chamber at 1.0 m from the x-ray source using a 50-μm-thick tungsten filter (Fig. 3). At a constant tube current, the x-ray intensity increased when the tube voltage was increased. At a tube voltage of 60 kV and a current of 0.10 mA, the intensity with the filter was 1.04 μGy/s.

3.2 Focal spot

In order to measure images of the x-ray source, we employed a pinhole camera with a hole diameter of 100 μm in conjunction with a Computed Radiography (CR) system with a sampling pitch of 87.5 μm (Fig. 4). When the tube voltage was increased using the filter, the spot diameter increased and had a maximum value of approximately 2.2 mm with a tube voltage of 70 kV.

3.3 X-ray spectra

In order to measure x-ray spectra, we employed a cadmium telluride detector (XR-100T, Amptek) (Fig. 5). Using the filter, low-photon-energy bremsstrahlung x-rays were absorbed, and sharp K lines were left. When the tube voltage was increased, the x-ray intensities of samarium K-series characteristic lines increased, and the maximum photon energy increased.

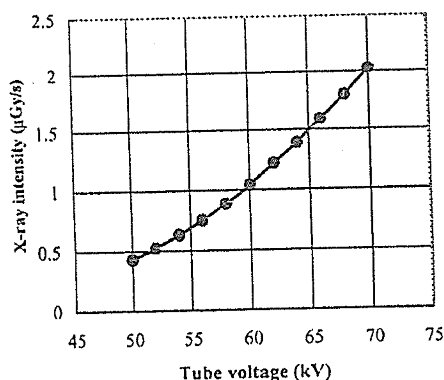

Fig. 3. X-ray intensity measured at 1.0 m from X-ray source according to changes in tube voltage using a tungsten filter.

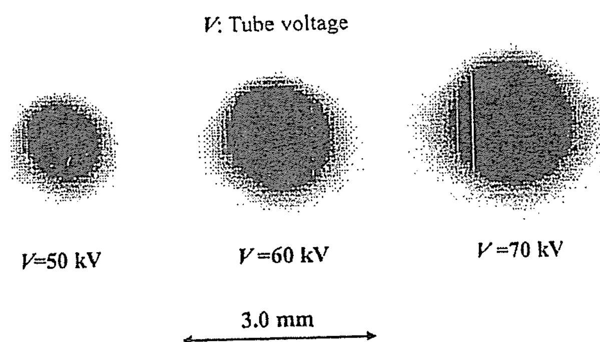

Fig. 4. Images of the x-ray source with changing the tube voltage.

4. K-EDGE ANGIOGRAPHY

Because the average photon energy of samarium Kα is 39.9 keV, iodine contrast media with a K-absorption edge of 33.2 keV absorb the Kα lines easily (Fig. 6). Therefore, blood vessels were observed with high contrasts. The angiography was performed using the CR system, iodine microspheres of 15 μm in diameter, and the filter. The distance between the x-ray source and the imaging plate was 1.0 m, and the tube voltage was 60 kV. First, rough measurements of spatial resolution were made using wires coiled around rods made of polymethyl methacrylate (PMMA) (Fig. 7). Although the image contrast decreased somewhat with decreases in the wire diameter, a 50-μm-diameter wire could be observed.

Figures 8 and 9 show angiograms of a rabbit heart and thigh, respectively. The coronary arteries in the heart and fine blood vessels in the thigh were visible. Figure 10 shows angiograms of a dog heart, and blood vessels of approximately 100 μm in diameter were observed.

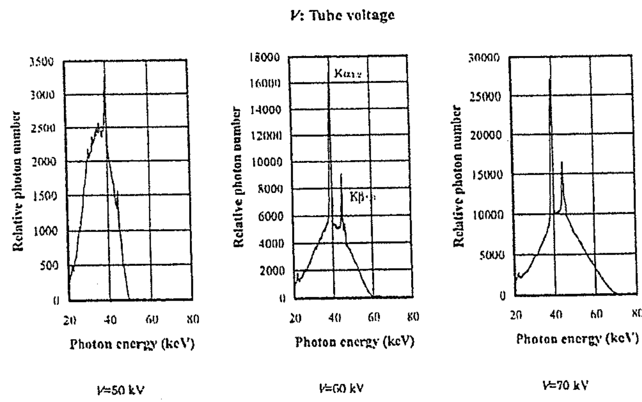

Fig. 5. X-ray spectra measured using a cadmium telluride detector with changes in tube voltage using the filter.

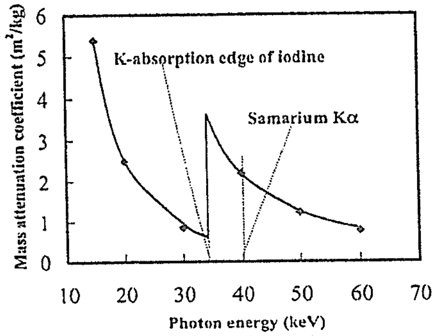

Fig. 6. Mass attenuation coefficients of iodine and average photon energy of samarium Kα lines.

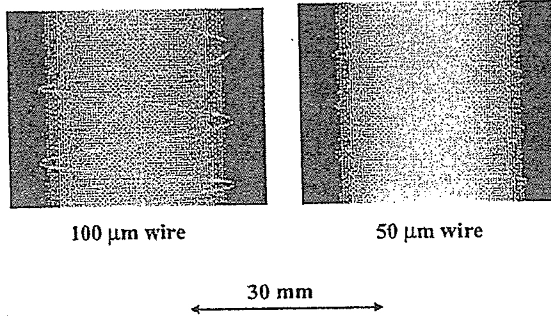

Fig. 7. Radiograms of tungsten wires coiled around PMMA rods.

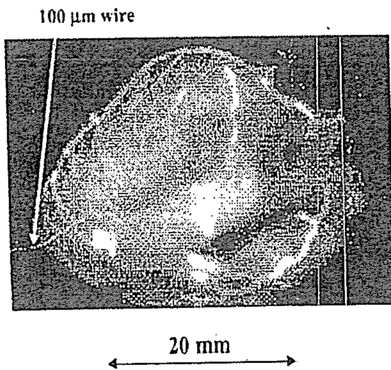

Fig. 8. Angiograms of an extracted rabbit heart using iodine microspheres.

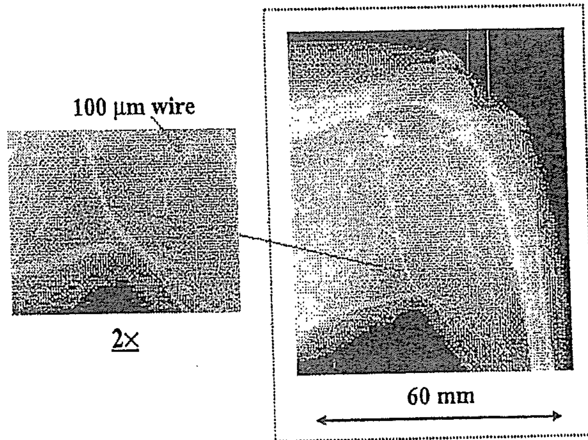

Fig. 9. Angiogram of a rabbit thigh using iodine microspheres.

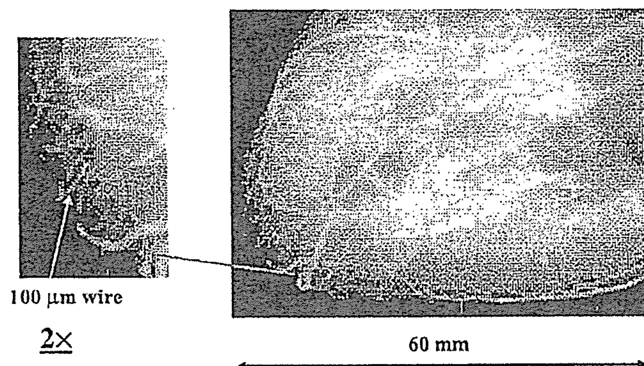

Fig. 10. Angiogram of an extracted dog heart using iodine microspheres.

5. DISCUSSION AND CONCLUSIONS

We employed an x-ray generator with a samarium-target tube and succeeded in producing samarium characteristic x-rays, which can be absorbed easily by iodine-based contrast media. Both the characteristic and bremsstrahlung x-ray intensities increased with increases in the tube voltage without filtering. Using the filter, K-rays were left by absorbing bremsstrahlung rays, and K-ray intensity increased with increases in the tube voltage.

Using this x-ray tube, we could produce K-series characteristic x-rays of nickel, copper, and molybdenum, and performed soft radiography. However it is difficult to produce clean samarium K-rays because bremsstrahlung x-ray intensity is in proportion to the atomic number. Therefore, optimum filters for absorbing bremsstrahlung rays should be employed to improve the image contrast of blood vessels.

Using the filter, the generator produced maximum number of characteristic photons was approximately 4×10^6 photons/($cm^2 \cdot$ s) at 1.0 m from the source, and the photon count rate can be increased easily by improving the target. For example, the rotation anode tube can be developed, and sufficient x-ray dose rates could be produced by increasing the anode diameter.

ACKNOWLEDGMENT

This work was supported by Grants-in-Aid for Scientific Research (13470154, 13877114, and 16591222) and Advanced Medical Scientific Research from MECSST, Health and Labor Sciences Research Grants (RAMT-nano-001, RHGTEFB-genome-005 and RHGTEFB-saisei-003), and grants from the Keiryo Research Foundation, Promotion and Mutual Aid Corporation for Private Schools of Japan, Japan Science and Technology Agency (JST), and New Energy and Industrial Technology Development Organization (NEDO, Industrial Technology Research Grant Program in '03).

REFERENCES

1. H. Mori, K. Hyodo, E. Tanaka, M. U. Mohammed, A. Yamakawa, Y. Shinozaki, H. Nakazawa, Y. Tanaka, T. Sekka, Y. Iwata, S. Honda, K. Umetani, H. Ueki, T. Yokoyama, K. Tanioka, M. Kubota, H. Hosaka, N. Ishizawa and M. Ando, "Small-vessel radiography in situ with monochromatic synchrotoron radiation," *Radiology*, **201**, 173-177, 1996.
2. K. Hyodo, M. Ando, Y. Oku, S. Yamamoto, T. Takeda, Y. Itai, S. Ohtsuka, Y. Sugishita and J. Tada, "Development of a two-dimensional imaging system for clinical applications of intravenous coronary angiography using intense synchrotron radiation produced by a multipole wiggler," *J. Synchrotron Radiat.*, **5**, 1123-1126, 1998.
3. E. Sato, Y. Hayasi, R. Germer, E. Tanaka, H. Mori, T. Kawai, T. Ichimaru, K. Takayama and H. Ido, "Quasi-monochromatic flash x-ray generator utilizing weakly ionized linear copper plasma," *Rev. Sci. Instrum.*, **74**,

5236-5240, 2003.
4. E. Sato, Y. Hayasi, R. Germer, E. Tanaka, H. Mori, T. Kawai, T. Ichimaru, S. Sato, K. Takayama and H. Ido, "Sharp characteristic x-ray irradiation from weakly ionized linear plasma," *J. Electron Spectrosc. Related Phenom.*, **137-140**, 713-720, 2004.
5. E. Sato, E. Tanaka, H. Mori, T. Kawai, S. Sato and K. Takayama, "Clean monochromatic x-ray irradiation from weakly ionized linear copper plasma," *Opt. Eng.*, **44**, 049002-1-6, 2005.
6. E. Sato, Y. Hayasi, R. Germer, E. Tanaka, H. Mori, T. Kawai, T. Inoue, A. Ogawa, S. Sato, K. Takayama, J. Onagawa, "X-ray spectra from weakly ionized linear copper plasma," *Jpn. J. Appl. Phys.*, **45**, 5301-5306, 2006.
7. E. Sato, E. Tanaka, H. Mori, T. Kawai, T. Inoue, A. Ogawa, S. Sato, K. Takayama and J. Onagawa, "Characteristic x-ray generator utilizing angle dependence of bremsstrahlung x-ray distribution," *Jpn. J. Appl. Phys.*, **45**, 2845-2849, 2006.
8. E. Sato, E. Tanaka, H. Mori, T. Kawai, T. Ichimaru, S. Sato, K. Takayama and H. Ido, "Demonstration of enhanced K-edge angiography using a cerium target x-ray generator," *Med. Phys*, **31**, 3017-3021, 2004.
9. E. Sato, A. Yamadera, E. Tanaka, H. Mori, T. Kawai, F. Ito, T. Inoue, A. Ogawa, S. Sato, K. Takayama, J. Onagawa and H. Ido, "X-ray spectra from a cerium target and their application to cone beam K-edge angiography," *Opt. Eng.*, **44**, 096502-1-6, 2005.
10. E. Sato, E. Tanaka, H. Mori, T. Kawai, T. Inoue, A. Ogawa, A. Yamadera, S. Sato, F. Ito, K. Takayama, J. Onagawa and H. Ido, "Variations in cerium x-ray spectra and enhanced K-edge angiography," *Jpn. J. Appl. Phys.*, **44**, 8204-8209, 2005.
11. E. Sato, K. Sato and Y. Tamakawa, "Film-less computed radiography system for high-speed imaging," *Ann. Rep. Iwate Med. Univ. Sch. Lib. Arts and Sci.*, **35**, 13-23, 2000.

*dresato@iwate-med.ac.jp; phone +81-19-651-5111; fax +81-19-654-9282

Japanese Journal of Applied Physics
Vol. 45, No. 4A, 2006, pp. 2845–2849
©2006 The Japan Society of Applied Physics

Characteristic X-ray Generator Utilizing Angle Dependence of Bremsstrahlung X-ray Distribution

Eiichi SATO, Etsuro TANAKA[1], Hidezo MORI[2], Toshiaki KAWAI[3], Takashi INOUE[4], Akira OGAWA[4], Shigehiro SATO[5], Kazuyoshi TAKAYAMA[6] and Jun ONAGAWA[7]

Department of Physics, Iwate Medical University, 3-16-1 Honchodori, Morioka 020-0015, Japan
[1]*Department of Nutritional Science, Faculty of Applied Bio-science, Tokyo University of Agriculture, 1-1-1 Sakuragaoka, Setagaya-ku, Tokyo 156-8502, Japan*
[2]*Department of Cardiac Physiology, National Cardiovascular Center Research Institute, 5-7-1 Fujishirodai, Suita, Osaka 565-8565, Japan*
[3]*Electron Tube Division #2, Hamamatsu Photonics K.K., 314-5 Shimokanzo, Iwata, Shizuoka 438-0193, Japan*
[4]*Department of Neurosurgery, School of Medicine, Iwate Medical University, 19-1 Uchimaru, Morioka 020-8505, Japan*
[5]*Department of Microbiology, School of Medicine, Iwate Medical University, 19-1 Uchimaru, Morioka 020-8505, Japan*
[6]*Shock Wave Research Center, Institute of Fluid Science, Tohoku University, 2-1-1 Katahira, Sendai 980-8577, Japan*
[7]*Department of Applied Physics and Informatics, Faculty of Engineering, Tohoku Gakuin University, 1-13-1 Chuo, Tagajo, Miyagi 985-8537, Japan*

(Received November 17, 2005; revised December 24, 2005; accepted December 31, 2005; published online April 7, 2006)

This generator consists of the following components: a constant high-voltage power supply, a filament power supply, a turbomolecular pump, and an X-ray tube. The X-ray tube is a demountable diode which is connected to the turbomolecular pump and consists of the following major devices: a molybdenum rod target, a tungsten hairpin cathode (filament), a focusing (Wehnelt) electrode, a polyethylene terephthalate X-ray window 0.25 mm in thickness, and a stainless-steel tube body. In the X-ray tube, the positive high voltage is applied to the anode (target) electrode, and the cathode is connected to the tube body (ground potential). In this experiment, the tube voltage applied was from 22 to 36 kV, and the tube current was regulated to within 100 μA by the filament temperature. The exposure time is controlled in order to obtain optimum X-ray intensity. The electron beams from the cathode are converged to the target by the focusing electrode, and clean K-series characteristic X-rays are produced through the focusing electrode without using a filter. The X-ray intensity was 26.6 μGy/s at 1.0 m from the X-ray source with a tube voltage of 30 kV and a tube current of 100 μA, and quasi-monochromatic radiography was performed using a computed radiography system. [DOI: 10.1143/JJAP.45.2845]

KEYWORDS: demountable X-ray tube, electron-impact source, quasi-monochromatic X-rays, K-series characteristic X-rays, Sommerfeld's theory

1. Introduction

A great deal of effort has been devoted to the research and development of X-ray lasers in past years, and several different generators have been developed. Using tera-watt pulse lasers as pumping sources, a transient collisional excitation method has been proposed.[1)] Subsequently, capillary discharge soft X-ray laser generators[2–4)] have been developed and demonstrated. However, it is difficult to produce high-photon-energy X-ray lasers with energies 10 keV or beyond.

Recently, we have developed several different flash X-ray generators[5–9)] corresponding to specific radiographic objectives, and the plasma X-ray source has been growing with increases in the electrostatic energy in the condenser. By forming weakly ionized linear plasma using rod targets, we confirmed irradiation of clean K-series characteristic X-rays such as hard X-ray lasers from the plasma axial direction using a table-top flash X-ray generator.[10–13)] This super fluorescence has been employed to perform cone-beam monochromatic radiography such as iodine K-edge and gadolinium K-edge angiographies. Furthermore, because higher harmonic hard X-rays have been produced from the copper plasma, we have to confirm the irradiations of higher harmonics with charges in the target element.

Without forming plasmas, demountable flash X-ray tubes can be employed to perform fundamental study on producing monochromatic X-rays,[14)] and have succeeded in producing clean K-series characteristic X-rays. However, monochromatic flash radiography has had difficulties in controlling X-ray duration, and in performing magnification radiography including phase-contrast effect.

At present, brilliant monochromatic parallel X-ray beams from synchrotron radiation are used in various fields including medical imaging,[15–17)] and large-scale X-ray free electron laser sources[18)] are constructing as a new-generation radiation source for producing monochromatic coherent X-rays. In contrast, small-scale steady-state monochromatic parallel and cone beams can be employed to perform medical imaging including phase-contrast radiography and K-edge angiography[19)] in hospitals.

In this paper, we developed an X-ray generator used to perform a preliminary experiment for generating clean K-series characteristic X-rays by angle dependence of the bremsstrahlung X-rays.

2. Generator

Figure 1 shows a block diagram of a compact characteristic (quasi-monochromatic) X-ray generator. This generator consists of the following components: a constant high-voltage power supply (SL150, Spellman), a DC filament power supply, a turbomolecular pump, and an X-ray tube. The structure of the X-ray tube is illustrated in Fig. 2. The X-ray tube is a demountable diode which is connected to the turbomolecular pump with a pressure of approximately 0.5 mPa and consists of the following major devices: a molybdenum rod target of 3.0 mm in diameter, a tungsten hairpin cathode (filament), a focusing (Wehnelt) electrode, a polyethylene terephthalate X-ray window 0.25 mm in thickness, and a stainless-steel tube body. In the X-ray tube, the positive high voltage is applied to the anode (target) electrode, and the cathode is connected to the tube body

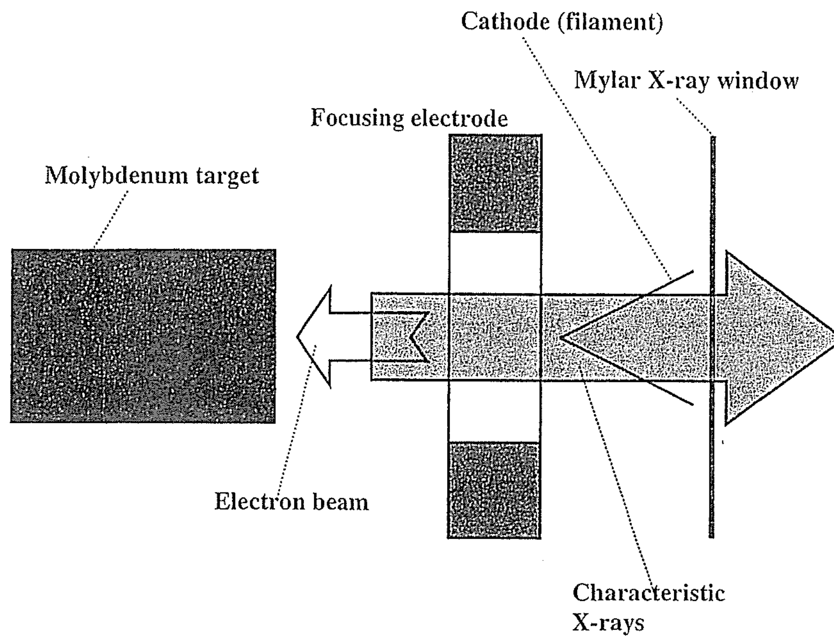

Fig. 3. K-photon irradiation from the X-ray tube.

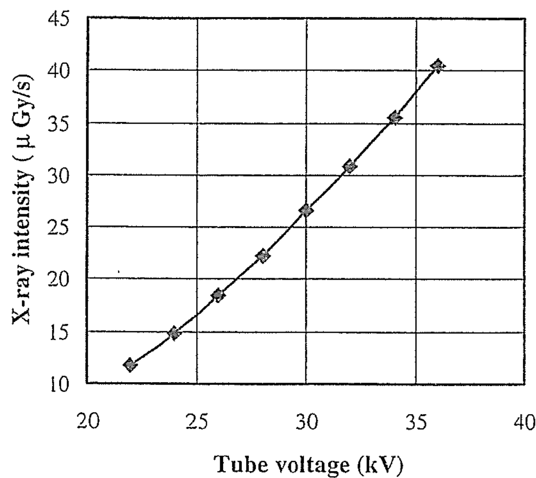

Fig. 4. X-ray intensity at 1.0 m from the X-ray source according to changes in the tube voltage with a tube current of 100 μA.

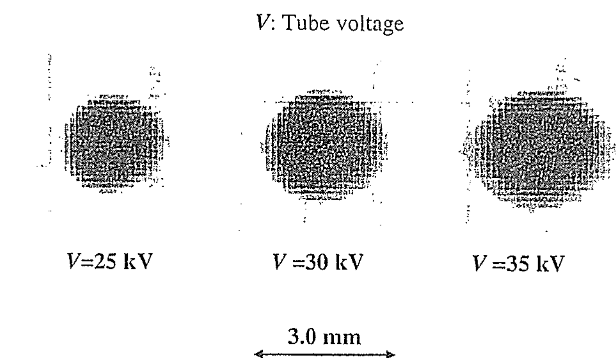

Fig. 5. Images of the characteristic X-ray source obtained using a pinhole camera with changes in the tube voltage.

detected by an imaging plate of the CR system (Konica Minolta, Regius 150) with a wide dynamic range, and relative X-ray intensity was calculated from Dicom original digital data corresponding to X-ray intensity; the data was scanned by Dicom viewer in the film-less CR system. Subsequently, the relative X-ray intensity as a function of the data was calibrated using a conventional X-ray generator, and we confirmed that the intensity was proportional to the exposure time. Figure 6 shows measured spectra from the molybdenum target. We observed clean K lines, while bremsstrahlung rays were hardly detected. The characteristic X-ray intensity substantially increased with increases in the tube voltage.

4. Radiography

The quasi-monochromatic radiography was performed by the CR system at 1.0 m from the X-ray source with the filter, and the tube voltage was 30 kV.

Firstly, rough measurements of image resolution were made using wires. Figure 7 shows radiograms of tungsten wires coiled around pipes made of poly(methyl methacrylate) (PMMA). Although the image contrast increased with increases in the wire diameter, a 50 μm-diameter wire could be observed.

A radiogram of a vertebra is shown in Fig. 8, and the fine structure of the vertebra was observed. Next, angiography was performed using iodine microspheres of 15 μm in diameter. Figures 9 and 10 show angiograms of a rabbit heart and thigh, respectively, and we could obtained high contrast images of coronary arteries and fine blood vessels.

5. Conclusions and Outlook

In summary, we developed a new quasi-monochromatic X-ray generator with a molybdenum-target tube and succeeded in producing clean molybdenum K lines. The characteristic X-ray intensity increased with increases in the tube voltage, and monochromatic Kα rays were left by a zirconium filter.

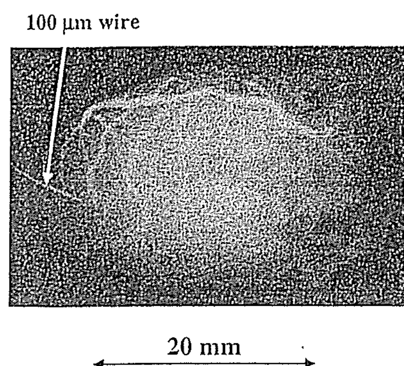

Fig. 9. Angiograms of a rabbit heart. Coronary arteries were visible.

Fig. 10. Angiogram of a rabbit thigh. Fine blood vessels of approximately 100 μm were visible.

the target evaporation. Subsequently, the generator produced maximum number of characteristic photons was approximately 1×10^8 photons/(cm^2·s) at 1.0 m from the source, and the photon count rate can be increased easily by increasing the current.

In the present research, the molybdenum K-series characteristic X-rays are useful for mammography, and the photon energies of characteristic X-rays can be selected by the target element. In particular, enhanced K-edge angiography can be performed using a cerium target because cerium Kα rays (34.6 keV) are absorbed easily by iodine-based contrast media with an iodine K-edge of 33.2 keV. Using this angiography, coronary arteries and fine blood vessels formed in regenerative medicine may be observed with high contrasts. Furthermore, a flat panel detector is useful to observe blood flows for cases of cardiovascular disease.

Acknowledgment

This work was supported by Grants-in-Aid for Scientific Research (13470154, 13877114, and 16591222) and Advanced Medical Scientific Research from MECSST, Grants from Keiryo Research Foundation, The Promotion and Mutual Aid Corporation for Private School of Japan, JST (Test of Fostering Potential), NEDO, and MHLW (HLSRG, RAMT-nano-001, RHGTEFB-genome-005, and RGCD13C-1).

1) K. Nagashima, M. Tanaka, M. Nishikino, M. Kishimoto, M. Kado, T. Kawachi, N. Hasegawa, Y. Ochi, K. Sukegawa, R. Tai and K. Kato: Proc. SPIE **5197** (2003) 1.
2) J. J. Rocca, V. Shlyaptsev, F. G. Tomasel, O. D. Cortazar, D. Hartshorn and J. L. A. Chilla: Phys. Rev. Lett. **73** (1994) 2192.
3) C. D. Macchietto, B. R. Benware and J. J. Rocca: Opt. Lett. **24** (1999) 1115.
4) J. J. G. Rocca, J. L. A. Chilla, S. Sakadzic, A. Rahman, J. Filevich, E. Jankowska, E. C. Hammarsten, B. M. Luther, H. C. Kapteyn, M. Murnane and V. N. Shlyapsev: Proc. SPIE **4505** (2001) 1.
5) E. Sato, S. Kimura, S. Kawasaki, H. Isobe, K. Takahashi, Y. Tamakawa and T. Yanagisawa: Rev. Sci. Instrum. **61** (1990) 2343.
6) K. Takahashi, E. Sato, M. Sagae, T. Oizumi, Y. Tamakawa and T. Yanagisawa: Jpn. J. Appl. Phys. **33** (1994) 4146.
7) E. Sato, K. Takahashi, M. Sagae, S. Kimura, T. Oizumi, Y. Hayasi, Y. Tamakawa and T. Yanagisawa: Med. Biol. Eng. Comput. **32** (1994) 289.
8) E. Sato, M. Sagae, K. Takahashi, A. Shikoda, T. Oizumi, Y. Hayasi, Y. Tamakawa and T. Yanagisawa: Med. Biol. Eng. Comput. **32** (1994) 295.
9) E. Sato, E. Tanaka, H. Mori, T. Kawai, T. Ichimaru, S. Sato, K. Takayama and H. Ido: Med. Phys. **32** (2005) 49.
10) E. Sato, Y. Hayasi, R. Germer, E. Tanaka, H. Mori, T. Kawai, T. Ichimaru, K. Takayama and H. Ido: Rev. Sci. Instrum. **74** (2003) 5236.
11) E. Sato, Y. Hayasi, R. Germer, E. Tanaka, H. Mori, T. Kawai, T. Ichimaru, S. Sato, K. Takayama and H. Ido: J. Electron Spectrosc. Relat. Phenom. C **137–140** (2004) 713.
12) E. Sato, E. Tanaka, H. Mori, T. Kawai, S. Sato and K. Takayama: Opt. Eng. **44** (2005) 049002.
13) E. Sato, R. Germer, E. Tanaka, H. Mori, T. Kawai, T. Ichimaru, S. Sato, H. Ojima, K. Takayama and H. Ido: Proc. SPIE **5580** (2005) 146.
14) E. Sato, M. Sagae, E. Tanaka, Y. Hayasi, R. Germer, H. Mori, T. Kawai, T. Ichimaru, S. Sato, K. Takayama and H. Ido: Jpn. J. Appl. Phys. **43** (2004) 7324.
15) A. Momose, T. Takeda, Y. Itai and K. Hirano: Nat. Med. **2** (1996) 473.
16) H. Mori *et al.*: Radiology **201** (1996) 173.
17) K. Hyodo, M. Ando, Y. Oku, S. Yamamoto, T. Takeda, Y. Itai, S. Ohtsuka, Y. Sugishita and J. Tada: J. Synchrotron Radiat. **5** (1998) 1123.
18) K. Lan, E. E. Fill and J. M. Vehn: Proc. SPIE **5197** (2003) 253.
19) E. Sato, E. Tanaka, H. Mori, T. Kawai, T. Ichimaru, S. Sato, K. Takayama and H. Ido: Med. Phys. **31** (2004) 3017.
20) B. K. Agarwal: *X-ray Spectroscopy* (Springer-Verlag, New York, 1991) 2nd ed., p. 18.
21) E. Sato, K. Sato and Y. Tamakawa: Annu. Rep. Iwate Med. Univ. School Lib. Arts Sci. **35** (2000) 13.

Cardiovasc Drugs Ther (2006) 20: 159–165
DOI 10.1007/s10557-006-8285-8

BASIC RESEARCH

Granulocyte Colony-Stimulating Factor Mediates Cardioprotection Against Ischemia/Reperfusion Injury via Phosphatidylinositol-3-Kinase/Akt Pathway in Canine Hearts

Hiroyuki Takahama · Tetsuo Minamino · Akio Hirata · Akiko Ogai · Hiroshi Asanuma · Masashi Fujita · Masakatsu Wakeno · Osamu Tsukamoto · Ken-ichiro Okada · Kazuo Komamura · Seiji Takashima · Yoshiro Shinozaki · Hidezo Mori · Naoki Mochizuki · Masafumi Kitakaze

Published online: 16 June 2006
© Springer Science + Business Media, LLC 2006

Abstract
Purpose Recent studies suggest that G-CSF prevents cardiac remodeling following myocardial infarction (MI) likely through regeneration of the myocardium and coronary vessels. However, it remains unclear whether G-CSF administered at the onset of reperfusion prevents ischemia/reperfusion injury in the acute phase. We investigated acute effects of G-CSF on myocardial infarct size and the incidence of lethal arrhythmia and evaluated the involvement of the phosphatidylinositol-3 kinase (PI3K) in the *in vivo* canine models.
Methods In open-chest dogs, left anterior descending coronary artery (LAD) was occluded for 90 minutes followed by 6 hours of reperfusion. We intravenously administered G-CSF (0.33 μ/kg/min) for 30 minutes from the onset of reperfusion. Wortmannin, a PI3K inhibitor, was selectively administered into the LAD after the onset of reperfusion.
Results G-CSF significantly ($p < 0.05$) reduced myocardial infarct size (38.7±4.3% to 15.7±5.3%) and the incidence of ventricular fibrillation during reperfusion periods (50% to 0%) compared with the control. G-CSF enhanced Akt phospholylation in ischemic canine myocardium. Wortmannin blunted both the infarct size-limiting and anti-arrhythmic effects of G-CSF. G-CSF did not change myeloperoxidase activity, a marker of neutrophil accumulation, in the infarcted myocardium.
Conclusion An intravenous administration of G-CSF at the onset of reperfusion attenuates ischemia/reperfusion injury through PI3K/Akt pathway in the *in vivo* model. G-CSF administration can be a promising candidate for the adjunctive therapy for patients with acute myocardial infarction.

Takahama and Hirata contributed equally to this work.

H. Takahama · A. Ogai · H. Asanuma · M. Wakeno · K. Komamura · H. Mori · M. Kitakaze
Department of Cardiovascular Medicine,
National Cardiovascular Center,
Suita 565-8565, Osaka, Japan

H. Takahama · M. Wakeno · N. Mochizuki
Department of Structural Analysis,
National Cardiovascular Center,
Suita 565-8565, Osaka, Japan

H. Takahama · M. Wakeno · N. Mochizuki
Department of Bioregulatory Medicine,
Osaka University Graduate School of Medicine,
Suita 565-0871, Osaka, Japan

T. Minamino (✉) · A. Hirata · M. Fujita · O. Tsukamoto · K.-i. Okada · S. Takashima
Department of Cardiovascular Medicine,
Osaka University Graduate School of Medicine,
2-2 Yamadaoka, Suita 565-0871, Osaka, Japan
e-mail: minamino@medone.med.osaka-u.ac.jp

Y. Shinozaki
Department of Physiological Science,
Tokai University School of Medicine,
Isehara 259-1193, Kanagawa, Japan

Key words G-CSF · myocardial infarction · ischemia-reperfusion injury · ventricular fibrillation · phosphatidylinositol-3 kinase · Akt

Abbreviations

VF ventricular fibrillation
G-CSF granulocyte colony-stimulating factor
WTMN wortmannin

Introduction

Granulocyte colony-stimulating factor (G-CSF), a 20-kDa glycoprotein, promotes the proliferation, survival and differentiation of hematopoietic cells [1]. Furthermore, G-CSF can mobilize hematopoietic stem cells from bone marrow [2, 3]. Thus, G-CSF is believed to improve cardiac remodeling after myocardial infarction (MI) through regeneration of the myocardium and angiogenesis [4, 5]. In addition to these effects of G-CSF, Komuro and colleagues clearly demonstrated that the high dose of G-CSF acutely reduces infarct size by preventing apoptosis in the isolated hearts [6]. However, it remains unclear whether clinically relevant dosages of G-CSF can reduce the infarct size in the in vivo model and, if so, it is not clear which downstream signaling pathway is involved in the acute cardioprotective effects of G-CSF. Furthermore, although lethal arrhythmias are a major cause of death in patients with acute myocardial infarction [7, 8], anti-arrhythmic effects of G-CSF have not been determined.

Thus, we investigated the acute effects of a clinical relevant dose of G-CSF on ischemia/reperfusion injury including both lethal arrhythmias and infarct size in canine hearts. We also examined a role of the PI3K/Akt pathway, a down stream of G-CSF receptors, in the cardioprotective effects of G-CSF. In the present study, we adopted ischemia/reperfusion protocols that have not been tested in previous studies [4, 5], because coronary revascularization has been established as a standard therapy to attenuate cardiac damage after MI.

Materials and methods

Materials

G-CSF was provided by Kirin brewery company (Tokyo, Japan). Recombinant human G-CSF can increase the number of white blood cells in dogs [9]. Wortmannin was obtained from Sigma (St. Louis, MO), and antibodies against Phospho-Akt and Akt were obtained from Cell signaling technologies (Beverly, MA).

Instrumentation

Twenty-nine beagle dogs (Kitayama Labes, Gifu, Japan) weighing 8 to 12 kg were anesthetized by an intravenous injection of sodium pentobarbital (30 mg/kg), intubated and ventilated with room air mixed with oxygen (100% O_2 at flow rate of 1.0 to 1.5 l/min). Thoracotomy was done at the fifth left intercostal space, and the heart was suspended in a pericardial cradle. After intravenous administration of heparin (500 U/kg), the left anterior descending coronary artery (LAD) was cannulated for perfusion with blood from the left carotid artery through an extracorporeal bypass tube. This allows the selective infusion of drugs into the LAD-perfused areas through this bypass tube. The left atrium was catheterized for microsphere injection to measure myocardial collateral blood flow during ischemia as described previously [10]. Hydration was maintained by a slow normal saline infusion. Both systemic blood pressure (SBP) and heart rate (HR) were monitored continuously during the study. All procedures were performed in conformity with the Guide for the care and use of laboratory animals (NIH Publication No. 85–23, 1996 revision), and were approved by the *Osaka University Committee for Laboratory Animal Use.*

Experimental protocols

Protocol 1. Acute effects of G-CSF on infarct size and lethal arrhythmias in canine hearts

After hemodynamic stabilization, we intravenously administered either saline (Control group; $n = 9$) or G-CSF (0.33 μg/kg/min) (G-CSF group; $n = 6$) for 30 min following the onset of reperfusion. An intracoronary administration of wortmannin (WTMN), a PI3K inhibitor, was selectively administered into the LAD (1.5 μg/kg/min) for 60 min after the onset of reperfusion (GCSF + WTMN group, $n = 7$; WTMN group, $n = 7$) (Fig. 1). We have previously confirmed that the dose of wortmannin used prevents the phosphorylation of Akt in myocardium [10]. We measured infarct size and myocardial collateral blood flow during ischemia. In brief, infarct size was evaluated at the end of the protocol by Evans blue/TTC staining. Collateral blood flow during 90 min of ischemia was assessed by the non-radioactive microsphere method [10]. We also counted

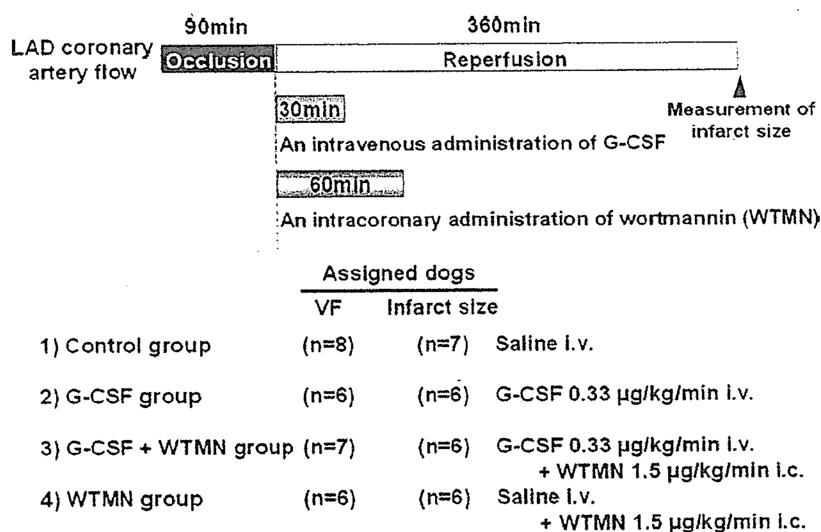

Fig. 1 Experimental protocols to assess myocardial infarct size and ventricular fibrillation (VF) in canine hearts. Myocardial infarct size was measured after 90 min of left anterior descending coronary artery (LAD) occlusion followed by 360 min of reperfusion. The incidence of VF was evaluated during reperfusion for 360 min. Intravenous administration of granulocyte colony-stimulating factor (G-CSF) was started at the onset of reperfusion and continued for 30 min. Intracoronary administration of wortmannin (WTMN) was started at the onset of reperfusion and continued for 60 min.

the incidence of VF during the 6 h reperfusion period (Fig. 1).

Finally, we measured myeloperoxidase (MPO) activity in LAD-perfused myocardium to check the accumulation of neutrophils in infarcted myocardium.

Protocol 2. Phosphorylation of Akt in ischemic myocardium

In this protocol, we used 11 dogs in Control group ($n = 3$), G-CSF group ($n = 4$), and G-CSF + WTMN group ($n = 4$). After 90 min of ischemia followed by 30 min of reperfusion, hearts were excised. The myocardial tissue in the ischemic zone, which was identified as the edge of the region showing necrosis, and non-ischemic zone were quickly placed into liquid nitrogen and stored at −80°C. Phosphorylation of Akt and total content of Akt were evaluated by immunoblotting as reported previously [10].

Immunoblotting

Immunoblotting was performed as described previously [11], and the immunoreactive bands were quantified by densitometry (Molecular Dynamics).

MPO activity

Several myocardial tissue samples were taken from the ischemic area in the dogs studied, frozen in liquid nitrogen and stored at −80°C until assay. The technical procedure has been described previously [12]. One unit of MPO activity was defined as that which degrades 1 μmol hydrogen peroxide per minute at 25°C.

Statistical analysis

Results are expressed as the mean ± SEM. Comparisons of the time course of the change in mean SBP and HR between groups were performed using two-way repeated measures analysis of variance (ANOVA). Comparisons of other data between groups were performed using one-way factional ANOVA. The Bonferroni-Holm procedure was used for correction of multiple comparisons [13]. The incidence of VF was compared using the χ^2-test and Fisher's exact probability test. A p value < 0.05 was considered to represent statistical significance.

Results

Criteria for exclusion

Since there was a negative correlation between myocardial collateral blood flow during ischemia and the incidence of VF [14, 15], it was important to assess myocardial collateral blood flow and exclude the dogs with high myocardial collateral blood flow. We excluded two dogs with excessive collateral blood flow (>15 ml/100 g/min) (Control group: 1, WTMN group: 1) among 29 dogs tested. Thus, 27 dogs were

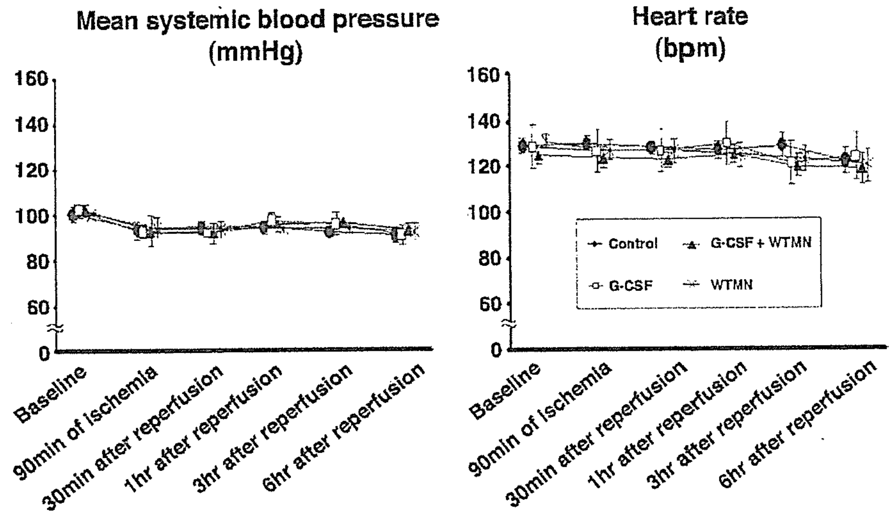

Fig. 2 The changes in mean systemic blood pressure (SBP) and heart rate (HR) during the experiment in groups tested. Neither SBP nor HR differed between the groups tested at baseline, 90 min of ischemia, at 30 min and 1, 3, and 6 h after reperfusion.

evaluated for VF analysis. Among these 27 dogs, we further excluded two dogs (Control group: 1, G-CSF + WTMN group: 1) from infarct size analysis that matched the exclusion criteria of lethal arrhythmia (more than two consecutive attempts required to convert VF with low-energy DC pulses applied directly to the heart) [10].

Effects of G-CSF on infarct size and VF during the reperfusion period

Throughout the study, neither SBP nor HR differed among the four groups (Fig. 2). The area at risk and myocardial collateral blood flow during myocardial ischemia were also comparable in the groups tested (Fig. 3). Figure 4 shows infarct size in the groups tested. G-CSF reduced ($p < 0.05$) infarct size compared with the control group. The intracoronary administration of wortmannin for 60 min after the onset of reperfusion abrogated the infarct size-limiting effects of G-CSF, although wortmannin alone did not affect infarct size.

G-CSF reduced ($p < 0.05$) the incidence of VF during the reperfusion period compared with the control group (Table 1). The antiarrhythmic effects of G-CSF were abolished by wortmannin.

Effect of G-CSF on MPO activity in infarcted myocardium

MPO activity in infarcted myocardium 6 h after reperfusion in G-CSF group did not differ from that in the control group. (10.0 ± 2.6 versus 10.7 ± 2.1 U/g protein).

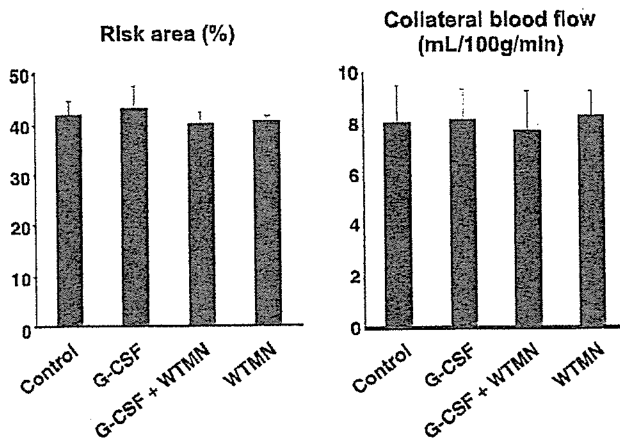

Fig. 3 Area at risk and myocardial collateral blood flow during ischemia in groups tested. Neither the area at risk nor myocardial collateral blood flow differed between the groups tested.

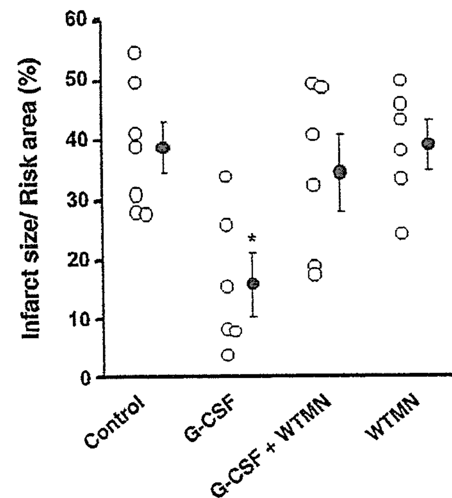

Fig. 4 Infarct size as a percentage of the area at risk in groups tested. Intravenous administration of G-CSF limited infarct size. The infarct-size limiting effect of G-CSF was blunted by the intracoronary administration of WTMN during reperfusion. *$p < 0.05$ vs. control group.

Table 1 Effects of G-CSF on the incidence of VF during reperfusion periods

Group	Incidence of VF (%)	
Control	50.0	(4/8)
G-CSF	0*	(0/6)
G-CSF + WTMN	42.9	(3/7)
WTMN	50.0	(3/6)

*$p < 0.05$ vs. control group

Effect of G-CSF on Akt phosphorylation in ischemic myocardium

G-CSF augmented Akt phosphrylation in the LAD-perfused myocardium. The increase in Akt phosphorylation was attenuated by wortmannin (Fig. 5).

Discussion

The present study demonstrated that administration of G-CSF following the onset of reperfusion limited infarct size in acute phase and reduced the incidence of lethal arrhythmia. The intracoronary administration of wortmannin abrogated these cardioprotective effects of G-CSF, suggesting that G-CSF mediated cardioprotection via the PI3K/Akt pathway. To our knowledge, this is the first study to reveal the acute effect of G-CSF against ischemia/reperfusion injury via the PI3K/Akt pathway in in vivo canine hearts.

Previous studies have reported that G-CSF improves cardiac remodeling after MI in the chronic ligation model of coronary artery [4, 5, 16]. It has been believed that G-CSF exerts cardioprotective effects through regenération of myocardium and angiogenesis. Recently, Komuro and colleagues clearly demonstrated that the high dose of G-CSF limits infarct size in the acute phase in the isolated hearts [6]. To translate their remarkable findings into the clinical setting, we need to consider the dose of G-CSF and experimental models in their study. They used a perfusate containing 300 ng/ml G-CSF in the isolated heart model. This dose is relatively high compared with the dose used in clinical settings [17, 18]. In addition, effects of G-CSF on neutrophil function cannot be tested in the isolated heart model. In the present study, we demonstrated that a clinical relevant dose of G-CSF acutely limits infarct size in the in vivo model. In contrast with previous studies [4, 5, 16], we examined the effects of G-CSF in the ischemia/reperfusion model, because coronary revascularization is principally applied for patients with acute MI to attenuate ischemia/reperfusion injury. We found that G-CSF following the onset of reperfusion effectively limited infarct size. Our findings strongly support that G-CSF would be a promising candidate as an adjunctive therapy for patients with acute MI. Indeed, two recent publications by the FIRSTLINE-AMI trial clearly demonstrated that subcutaneous administration of G-CSF after percutaneous coronary intervention improved cardiac function and prevented cardiac remodeling [19, 20]. Considering our present data, the improvement of cardiac function by G-CSF in clinical studies will be due to limiting infarct size in the acute phase as well as preventing cardiac remodeling.

G-CSF can provoke multiple intracellular signal transductions including Jak/Stat, ERK and PI3K/Akt [16, 21]. Recently, we and others demonstrated that post-interventions which activate PI3K/Akt during the reperfusion protect against ischemia/reprfusion injury [10, 22]. Thus, we investigated a role of PI3K/Akt in G-CSF-mediated cardioprotection. WTMN significantly blunted the infarct size-limiting effects of G-CSF, and G-CSF enhanced Akt phosphorylation in the ischemic myocardium, indicating that G-CSF reduces infarct size via PI3K/Akt-dependent pathway. Further investigations will be needed to clarify the molecular target of PI3K/Akt and the role of other signals activated by G-CSF in this condition.

Although we demonstrated that G-CSF mediated cardioprotection, one small clinical study showed that G-CSF may induce coronary re-stenosis [23]. In contrast, other large-scale studies did not show that G-CSF induced coronary restenosis [19, 20]. Since there is still controversy about the restenosis effects of G-

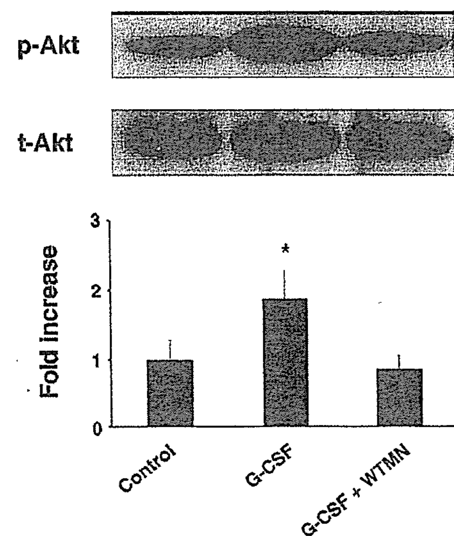

Fig. 5 Akt phosphorylation in LAD-perfused areas. G-CSF phosphorylated Akt in LAD-perfused myocardium. Akt phosphorylation by G-CSF was prevented by co-treatment with WTMN. Akt phosphorylation was normalized by total Akt. *$p < 0.05$ vs. control group.

CSF, this issue will be minimized by the concomitant use of a drug-eluting stent and G-CSF. Another possible adverse effect of G-CSF will be enhancement of neutrophil function. G-CSF appears not only to stimulate the formation of granulocyte colonies from bone marrow-derived precursors, but also to enhance the function of mature neutrophils [24] and elevates the number of white blood cells, which may predict adverse prognosis in the patients of acute MI [25]. Consistent with previous studies [26, 27], we also showed that G-CSF did not change MPO activity, a marker of neutrophil accumulation, in the infarcted myocardium. These findings suggest that G-CSF exerted cardioprotective effects independent of white blood cells. Although our findings suggest that the overall effect of G-CSF may be beneficial for ischemia/reperfused myocardium, we need to be cautious about these potential adverse effects of G-CSF.

Importantly, we clearly demonstrated that G-CSF reduced the incidence of VF during reperfusion via the PI3/Akt-dependent pathway. Since lethal arrhythmias are one of the major causes of death in patients with acute MI [8], the anti-arrhythmic effects of G-CSF have great clinical impact. We have previously demonstrated that another cytokine, erythropoietin, also reduced the incidence of lethal arrhythmia via the PI3/Akt pathway [10]. Although our findings suggest that the PI3K/Akt-dependent pathway will play an important role in the generation of lethal arrhythmias, further investigation will be needed to clarify the potential mechanism by which G-CSF exerts anti-arrhythmic effects. We need to consider whether G-CSF exerts anti-arrhythmic effects by the reduction of myocardial infarct size or by some other actions of G-CSF.

In conclusion, the intravenous administration of a clinically relevant dose of G-CSF will be a promising strategy to treat patients with acute MI. Further controlled studies will be warranted to check the safety and efficacy of G-CSF treatment in the acute phase after MI.

Acknowledgments We thank Yuko Okuda, and Yoko Nagamachi for their technical assistance.

References

1. Clark SC, Kamen R. The human hematopoietic colony-stimulating factors. Science 1987;236:1229–37.
2. To LB, Haylock DN, Simmons PJ, Juttner CA. The biology and clinical uses of blood stem cells. Blood 1997;89:2233–58.
3. Kronenwett R, Martin S, Haas R. The role of cytokines and adhesion molecules for mobilization of peripheral blood stem cells. Stem Cells 2000;18:320–30.
4. Orlic D, Kajstura J, Chimenti S, et al. Mobilized bone marrow cells repair the infarcted heart, improving function and survival. Proc Natl Acad Sci USA 2001;98:10344–9.
5. Ohtsuka M, Takano H, Zou Y, et al. Cytokine therapy prevents left ventricular remodeling and dysfunction after myocardial infarction through neovascularization. Faseb J 2004;18:851–3.
6. Harada M, Qin Y, Takano H, et al. G-CSF prevents cardiac remodeling after myocardial infarction by activating the Jak-Stat pathway in cardiomyocytes. Nat Med 2005;11:305–11.
7. Nicod P, Gilpin E, Dittrich H, et al. Late clinical outcome in patients with early ventricular fibrillation after myocardial infarction. J Am Coll Cardiol 1988;11:464–70.
8. Rouleau JL, Talajic M, Sussex B, et al. Myocardial infarction patients in the 1990s—their risk factors, stratification and survival in Canada: the Canadian Assessment of Myocardial Infarction (CAMI) Study. J Am Coll Cardiol 1996;27:1119–27.
9. Lothrop CD Jr, Warren DJ, Souza LM, Jones JB, Moore MA. Correction of canine cyclic hematopoiesis with recombinant human granulocyte colony-stimulating factor. Blood 1988;72:1324–8.
10. Hirata A, Minamino T, Asanuma H, et al. Erythropoietin just before reperfusion reduces both lethal arrhythmias and infarct size via the phosphatidylinositol-3 kinase-dependent pathway in canine hearts. Cardiovasc Drugs Ther 2005;19:33–40.
11. Maruyama R, Takemura G, Aoyama T, et al. Dynamic process of apoptosis in adult rat cardiomyocytes analyzed using 48-hour videomicroscopy and electron microscopy: beating and rate are associated with the apoptotic process. Am J Pathol 2001;159:683–91.
12. Asanuma H, Kitakaze M, Funaya H, et al. Nifedipine limits infarct size via NO-dependent mechanisms in dogs. Basic Res Cardiol 2001;96:497–505.
13. Holm S. A simple sequentially rejective multiple test procedure. Scand J Statist 1979;6:65–70.
14. Hale SL, Lange R, Alker KJ, Kloner RA. Correlates of reperfusion ventricular fibrillation in dogs. Am J Cardiol 1984;53:1397–400.
15. Bolli R, Patel B. Factors that determine the occurrence of reperfusion arrhythmias. Am Heart J 1988;115:20–9.
16. Iwanaga K, Takano H, Ohtsuka M, et al. Effects of G-CSF on cardiac remodeling after acute myocardial infarction in swine. Biochem Biophys Res Commun 2004;325:1353–9.
17. Gabrilove JL, Jakubowski A, Fain K, et al. Phase I study of granulocyte colony-stimulating factor in patients with transitional cell carcinoma of the urothelium. J Clin Invest 1988; 82:1454–61.
18. Bensinger WI, Clift RA, Anasetti C, et al. Transplantation of allogeneic peripheral blood stem cells mobilized by recombinant human granulocyte colony stimulating factor. Stem Cells 1996;14:90–105.
19. Ince H, Petzsch M, Kleine HD, et al. Prevention of left ventricular remodeling with granulocyte colony-stimulating factor after acute myocardial infarction: final 1-year results of the Front-Integrated Revascularization and Stem Cell Liberation in Evolving Acute Myocardial Infarction by Granulocyte Colony-Stimulating Factor (FIRSTLINE-AMI) Trial. Circulation 2005;112:I73–80.
20. Ince H, Petzsch M, Kleine HD, et al. Preservation from left ventricular remodeling by front-integrated revascularization and stem cell liberation in evolving acute myocardial infarction by use of granulocyte-colony-stimulating factor (FIRSTLINE-AMI). Circulation 2005;112:3097–106.
21. Avalos BR. Molecular analysis of the granulocyte colony-stimulating factor receptor. Blood 1996;88:761–77.

22. Tsang A, Hausenloy DJ, Mocanu MM, Yellon DM. Postconditioning: a form of "modified reperfusion" protects the myocardium by activating the phosphatidylinositol 3-kinase-Akt pathway. Circ Res 2004;95:230–2.
23. Kang HJ, Kim HS, Zhang SY, et al. Effects of intracoronary infusion of peripheral blood stem-cells mobilised with granulocyte-colony stimulating factor on left ventricular systolic function and restenosis after coronary stenting in myocardial infarction: the MAGIC cell randomised clinical trial. Lancet 2004;363:751–6.
24. Weisbart RH, Golde DW, Clark SC, Wong GG, Gasson JC. Human granulocyte-macrophage colony-stimulating factor is a neutrophil activator. Nature 1985;314:361–3.
25. Barron HV, Cannon CP, Murphy SA, Braunwald E, Gibson CM. Association between white blood cell count, epicardial blood flow, myocardial perfusion, and clinical outcomes in the setting of acute myocardial infarction: a thrombolysis in myocardial infarction 10 substudy. Circulation 2000;102: 2329–34.
26. Adachi Y, Imagawa J, Suzuki Y, et al. G-CSF treatment increases side population cell infiltration after myocardial infarction in mice. J Mol Cell Cardiol 2004;36: 707–10.
27. Sugano Y, Anzai T, Yoshikawa T, et al. Granulocyte colony-stimulating factor attenuates early ventricular expansion after experimental myocardial infarction. Cardiovasc Res 2005;65:446–56.

Summary: An amphiphilic poly(*N*-propargylamide) with galactose and lauryloyl groups was synthesized by copolymerization of the corresponding *N*-propargylamide monomers using a Rh catalyst. The obtained copolymer formed a one-handed helical conformation and molecular aggregates in water. The observations by fluorescence microscopy in a cell culture experiment in the presence of dye-labeled copolymer indicated that the copolymer was incorporated into the cells.

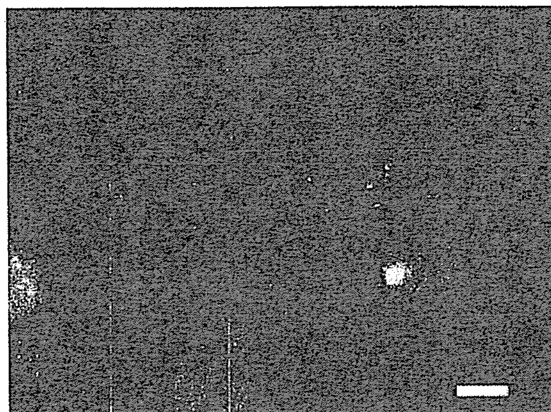

Localization of rhodamine B-labeled copolymer **8** in human aortic endothelial cells (fluorescence image).

Amphiphilic Poly(*N*-propargylamide) with Galactose and Lauryloyl Groups: Synthesis and Properties

Masakazu Suenaga,[1] *Yoshiro Kaneko,*[1] *Jun-ichi Kadokawa,**[1] *Takehiro Nishikawa,*[2] *Hidezo Mori,*[2] *Masayoshi Tabata*[3]

[1] Department of Nanostructured and Advanced Materials, Graduate School of Science and Engineering, Kagoshima 890-0065, Japan
Fax: +81-99-285-3253; E-mail: kadokawa@eng.kagoshima-u.ac.jp
[2] National Cardiovascular Center, Suita, Osaka 565-8565, Japan
[3] Department of Molecular Chemistry, Graduate School of Engineering, Hokkaido University, Sapporo 060-8628, Japan

Received: July 19, 2006; Accepted: October 10, 2006; DOI: 10.1002/mabi.200600228

Keywords: amphiphiles; conjugated polymers; copolymerization; dynamic light scattering; nanoparticles; polyacetylenes

Introduction

Synthesis of polymers having sugar residues, so-called glycopolymers, has been widely investigated to seek biological applications because of their versatile functions.[1] It has been demonstrated that these glycopolymers can bind specifically to carbohydrate-recognition proteins, toxins, viruses, and cells, and, thus, these polymers can be utilized as cell culture substrates with specific cell recognition sites, as well as in targeting drug delivery systems.[2] The clustered saccharide ligands conjugated to the polymeric main chains are involved in these specific recognition processes. Most of the previously prepared glycopolymers have been based on a flexible polymer backbone, such as polystyrene and polyacrylamide.[3,4] This flexible nature of the glycopolymers causes the disordered orientation of the sugar residues in the glycopolymers. Regular orientation of the sugar residues is necessary for efficient interaction between the glycopolymers and receptor molecules. In this sense, the spatially regulated orientation of the sugar residues should be realized by attaching the sugar residues to a polymer backbone with a rigid conformation. The sugar residues attached to the rigid polymer backbone may give rise to the ordered orientation that can improve the molecular recognition of sugar residues by specific cell receptors. This is because the spatial regulation of the sugar residues is significant in molecular recognition as well as the chemical structure of the sugar molecules.[5]

WILEY InterScience DISCOVER SOMETHING GREAT

© 2006 WILEY-VCH Verlag GmbH & Co. KGaA, Weinheim

From the above viewpoints, rigid glycopolymers with π-conjugated polymer backbones would be a novel type of bio-inspired polymers, which could exhibit multiple valence states and interact specifically and firmly with targets such as cell surface receptors and biomacromolecules. In some previous works, rigid glycopolymers having various π-conjugated main chains, such as polythiophene,[6] poly(*p*-phenylene ethynylene),[7] polyisocyanide,[8] polyaniline,[9] poly(*p*-phenylene vinylene),[10] and poly(phenylacetylene), have already been synthesized.[11] In the series of these studies, we reported the synthesis of poly(*N*-propargylamide) (2) with sugar residues. It contained a *cis*-polyacetylene main chain and was obtained by the rhodium-catalyzed polymerization of a *N*-propargylamide monomer (1) that had a galactose residue (Scheme 1).[12] Since polymerizations of the *N*-propargylamide monomers having various substituted groups using Rh catalyst have been widely reported to produce the corresponding poly(*N*-propargylamide) derivatives with *cis*-isomers,[13] we also investigated the copolymerization of 1 with *N*-propargylamide derivative 3 having a hexanoyl group to produce the amphiphilic glycopolymer 4, as shown in Scheme 1. We tested the solubility of copolymer 4 in various solvents to confirm whether the copolymer exhibits an amphiphilic property. Although the homopolymer 2 is insoluble in common organic solvents, the copolymer 4 can be dissolved in some polar organic solvents, such as dimethyl sulfoxide (DMSO) and *N,N*-dimethylformamide (DMF), as well as in aqueous medium. However, the copolymer still exhibits a hydrophilic nature rather than an amphiphilic nature. We assumed that insufficient amphiphilicity of copolymer 4 could be attributed to poor hydrophobic property of the hydrophobic part.

In this study, we chose a more hydrophobic monomer: *N*-propargylamide monomer 5 having a longer alkyl chain, i.e., the lauryloyl group, as the hydrophobic part of the amphiphilic copolymer. The monomer 5 was copolymerized with 1 in the presence of Rh catalyst to give the corresponding amphiphilic copolymer 6 (Scheme 2). The resulting copolymer 6 can be expected to have the ability to conduct molecular aggregation in water, which is driven by intermolecular and intramolecular association of the hydrophobic lauryloyl groups.

We believe that such molecular aggregates of the amphiphilic copolymer should play a significant role in the field of targeted drug delivery. The idea is supported by the following characteristics of the molecular aggregates:

1) Drug carriers with nanometer dimensions can be obtained by molecular aggregation of amphiphilic copolymers.
2) Nano-sized aggregates can remain in the bloodstream for an extended period because of the size-dependent uptake in the reticuloendothelial system.
3) Drug molecules with hydrophobic natures can be loaded into hydrophobic milieus formed by the association of hydrophobic long alkyl chains; otherwise the drug molecules could be directly attached to the constituent monomer molecules of the copolymer.
4) Sugar residues of the copolymer can function as recognition sites for target cells and tissues as well as providing the hydrophilic character of the amphiphilic copolymer.

Therefore, we studied the *in vitro* cell uptake of the molecular aggregates of the amphiphilic copolymer. For this purpose, the fluorescent marker, rhodamine B, was introduced into the amphiphilic copolymer. In this article, we report the synthesis of the amphiphilic

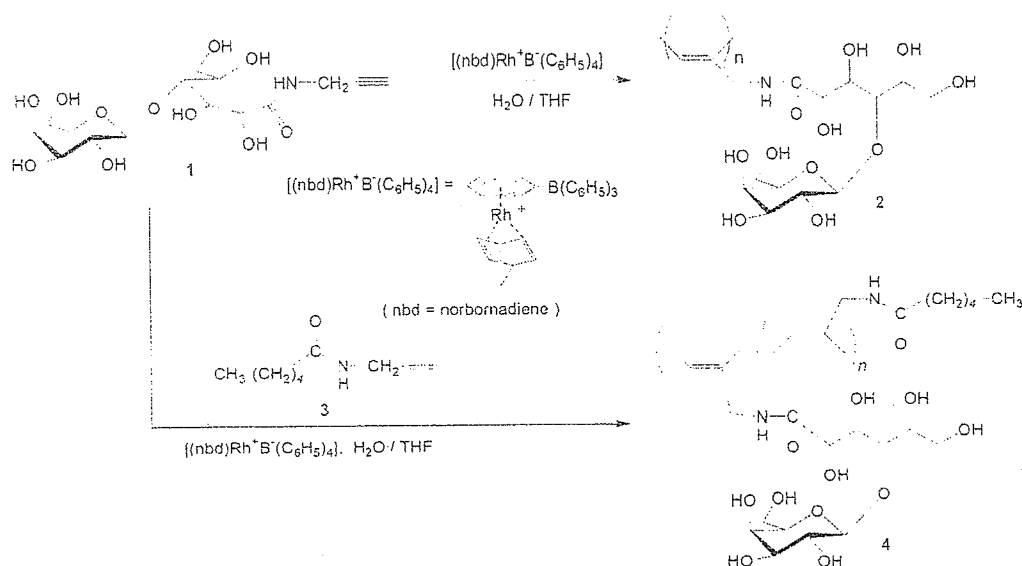

Scheme 1. Polymerization of 1 and copolymerization of 1 with 3.

© 2006 WILEY-VCH Verlag GmbH & Co. KGaA, Weinheim

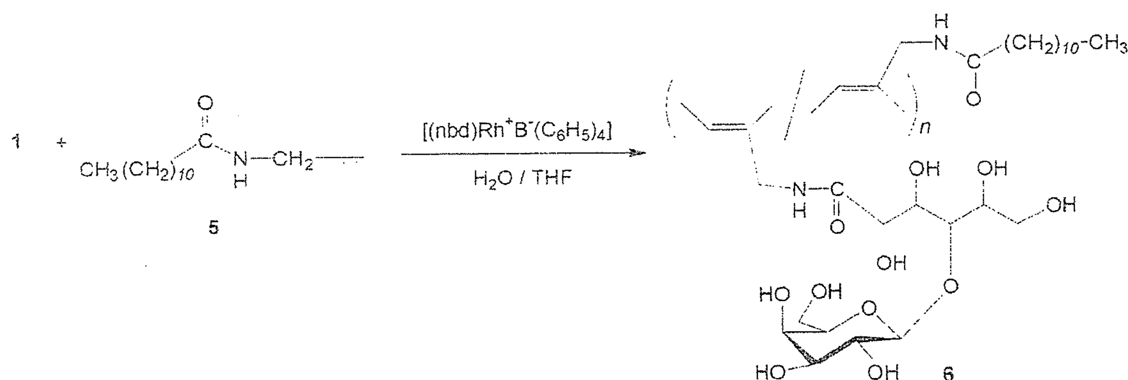

Scheme 2. Copolymerization of 1 with 5.

poly(*N*-propargylamide) 6 by Rh-catalyzed copolymerization, evaluation of its molecular aggregation in water [gel permeation chromatography (GPC) characterization, scanning electron microscopy (SEM) observation, and dynamic light scattering (DLS) measurement] and secondary conformation [circular dichroism (CD) spectra], and cell uptake of the nanoaggregate of the rhodamine-labeled amphiphilic copolymer (fluorescence microscopy).

Experimental Part

Materials

Monomer 1 and catalyst $(nbd)Rh^+B^-(C_6H_5)_4$ were prepared according to the literature.[12,14] Tetrahydrofuran (THF) used as polymerization solvent was purified by distillation. Other reagents and solvents were used as received without further purification.

Synthesis of Monomer 5

Monomer 5 was synthesized by a method similar to that used for 3.[15] Under argon, *N*-propargylamine hydrochloride (0.915 g, 10.0 mmol) was dissolved by slight warming in anhydrous acetonitrile (12.0 mL), and triethylamine (3.35 mL, 24.0 mmol) was added to the solution at room temperature. Then a solution of lauryloyl chloride (2.36 mL, 10.0 mmol) in anhydrous acetonitrile (12.0 mL) was added dropwise to the solution. After the mixture was stirred for 2 h, the reaction solution was concentrated by evaporation. The residue was dissolved in ethyl acetate and the solution was washed successively three times with 2 mol · L^{-1} hydrochloric acid and with saturated $NaHCO_3$ aqueous solution. The organic layer was dried over anhydrous Na_2SO_4, filtered, and evaporated. The residue was subjected to column chromatography on silica gel (hexane:ethyl acetate = 4:1, v/v) to isolate 5 (1.38 g, 5.82 mmol) in 58.2% yield.

^{1}H NMR ($CDCl_3$): δ = 0.88 (t, J = 7.2 Hz, CH_3, 3H), 1.28 [m, $CH_3(CH_2)_8$, 16H], 1.62 (m, $CH_2CH_2C{=}O$, 2H), 2.19 (t, J = 7.8 Hz, $CH_2C{=}O$, 2H), 2.23 (t, J = 2.4 Hz, H–C≡C, 1H), 4.05–4.06 (m, CH_2N, 2H), 5.57 (s, NH, 1H).

Synthesis of Monomer 7

Under argon, triethylamine (0.836 mL, 6.00 mmol) was added to a solution of *N*-propargylamine hydrochloride (0.549 g, 6.00 mmol) and rhodamine B (1.92 g, 4.0 mmol) in anhydrous methanol (10.0 mL) at 0 °C. To the solution was added 1-[(3-dimethylamino)propyl]-3-ethylcarbodiimide hydrochloride (1.15 g, 6.00 mmol) as a condensing agent at 0 °C and the mixture was stirred for 17 h at room temperature. The precipitated material was isolated by filtration and dried under the reduced pressure to give 7 (0.472 g, 0.915 mmol) in 23.0% yield.

^{1}H NMR ($CDCl_3$): δ = 1.16 (m, CH_3, 12H), 1.77 (t, J = 2.4 Hz, H–C≡C, 1H), 3.33 (m, NCH_2CH_3, 8H), 3.95 (d, J = 1.8 Hz, $CH_2C{\equiv}$, 2H), 6.26–7.93 (m, aromatics, 10H).

Copolymerization of 1 with 5

A typical copolymerization procedure was as follows (entry 1, Table 1). Under argon, a solution of 5 (0.0356 g, 0.150 mmol) in THF (0.90 mL) and a solution of catalyst (0.00630 g, 0.0125 mmol) in THF (0.90 mL) were added to a solution of 1 (0.0397 g, 0.100 mmol) in water (0.20 mL) in this order at 30 °C. After the mixture was stirred at 30 °C for 140 min, the reaction mixture was concentrated by evaporation and dried under reduced pressure. The residue was dissolved in a small amount of DMSO and the solution was poured into a large amount of methanol to precipitate the polymeric product. The precipitate was isolated by filtration and was dried under reduced pressure to give 6 (0.0588 g) in 78.1% yield.

^{1}H NMR (DMSO-d_6): δ = 0.84 (CH_3), 1.21 [$CH_3(CH_2)_8$], 1.45 ($CH_2CH_2C{=}O$), 2.15 ($CH_2C{=}O$), 3.0–3.9 [–CH(O–D-gal)–CH(OH)–CH_2OH, =CCH_2–, H2–H6 of D-gal], 4.04 [C(=O)CH(OH)CH(OH)–], 4.29 [C(=O)CH(OH)– and H1(β) of D-gal], 4.55, 4.79, 5.22 (OH), 6.11 (–CH=C–), 7.93 (NH).

Copolymerization of 1, 5, and 7

Under argon, a solution of 5 (0.0285 g, 0.120 mmol) and 7 (0.0929 g, 0.180 mmol) in THF (0.90 mL) and a solution of catalyst (0.0166 g, 0.0330 mmol) in THF (0.90 mL) were

© 2006 WILEY-VCH Verlag GmbH & Co. KGaA, Weinheim

Table 1. Results for copolymerization of **1** with **5** with Rh catalyst in THF–water (9:1) solvent.

Entry	Feed ratio[a]	Time	Yield[b]	Unit ratio[c]	$\overline{M}_n$[d]	$\overline{M}_w/\overline{M}_n$[d]	$[\alpha]_D$[e]
	1:**5**	min	%	**1**:**5**			degrees
1	1.0:1.5	140	78.1	1.0:0.92	9 100	1.30	–
2	1.0:1.0	195	62.5	1.0:0.88	6 200	1.63	–
3	1.0:0.67	240	57.0	1.0:0.35	5 200	1.60	−96.8
4	1.0:0.50	260	68.9	1.0:0.32	9 600	1.64	−142.3
5	1.0:0.33	200	69.9	1.0:0.26	7 100	1.50	−173.6
6	1.0:0.20	210	78.1	1.0:0.17	9 700	1.30	185.6

[a] [Catalyst]/[1 + 5] = 0.05, reaction temperature: 30 °C.
[b] Fraction insoluble in methanol.
[c] Determined from ^{1}H NMR spectra.
[d] Determined by GPC with water as eluent using pullulan standards, sample concentration = 0.1 mg · mL^{-1}.
[e] Measured by polarimetry in water, c = 1.0 g · dL^{-1} at 20 °C.

added to a solution of **1** (0.143 g, 0.360 mmol) in water (0.20 mL) in this order at 30 °C. After the mixture was stirred at 30 °C for 18 h, the reaction mixture was concentrated by evaporation and dried under reduced pressure. The residue was dissolved in a small amount of DMSO and the solution was poured into a large amount of methanol to precipitate the polymeric product. The precipitate was isolated by filtration and dried under reduced pressure to give **8** (0.164 g) in 62.0% yield.

^{1}H NMR (DMSO-d_6 – D_2O): δ = 0.93 ($CH_3CH_2CH_2$), 1.16 (CH_3CH_2N), 1.25 [$CH_3(CH_2)_8$], 1.50 ($CH_2CH_2C{=}O$), 3.0–4.5 (sugar protons and =C–CH_2), 6.16 (HC=), 7.0–8.0 (aromatics).

Cell Culture Experiment

Human aortic endothelial cells (HAECs) were purchased as cryopreserved samples of third passage (Lot: 3F1346) from Cambrex (Wakersville, MD, USA). The HAECs were subcultured once and stored in liquid nitrogen until cell culture experiment. The HAECs used in the experiment were fourth passage. Each well of a 12-well plate of polystyrene (Iwaki) was filled with 1 mL of a supplemented culture medium (EGM-2; Lot: 08103123, Cambrex) and equilibrated at 37 °C in a humidified incubator under 5% CO_2 for 30 min before cell seeding. After the frozen cells were thawed at 37 °C, 10 μL of the cell suspension was seeded in each well. The initial cell density was 2.2 × 10^3 cells · cm^{-2}. Cell viability assessed by the trypan blue exclusion test was 83% for the cell suspension. The cell seeded plates were placed in a humidified incubator at 37 °C under 5% CO_2. The HAECs were cultured for 48 h. Cell culture mediums were replaced with fresh medium 24 h after cell seeding. At 48 h after cell seeding, cell culture mediums were each replaced with an aqueous suspension of copolymer **8**. Then the HAECs were cultured in the polymer suspension for 1, 6, and 24 h in a humidified incubator at 37 °C under 5% CO_2 to study cellular uptake of nanoaggregates of copolymer **8**. For fluorescence microscopy observation, the cells were fixed by immersion in 10% formaldehyde neutral buffer solution (Nacalai Tesque) at room temperature (22 °C) for 15 min and were washed three times with phosphate-buffered saline (PBS; Gibco). Fluorescence images of the cells were taken with a fluorescence microscope (IX71; Olympus) equipped with a CCD camera (DP70; Olympus). Fluorescence intensity of the incorporated copolymer **8** was measured by integrating the fluorescence intensity observed at each pixel of the fluorescence images using image analysis software (Fluoview ver. 5.0; Olympus).

Measurements

NMR spectra were recorded on a JEOL ECA 600 spectrometer. Optical rotations were measured with a Jasco P-1030 digital polarimeter. GPC analyses were performed by using a TOSOH 8012 with refractive index detection under the following conditions: Shodex Asahipak GF-310HQ column with water as eluent at a flow rate of 0.5 mL · min^{-1}. The calibration curve was obtained using pullulan standards. CD and UV-vis spectra were measured in a quartz cell (thickness 1 cm) at room temperature using a Jasco J-820 spectropolarimeter and Shimadzu UV160A spectrophotometer, respectively. The SEM images were obtained using a Hitachi S-4100 electron microscope. The DLS measurement was performed on a Zetasizer 3000 (Malvern Instruments). Fluorescence spectra were obtained on a fluorescence spectrometer (Shimadzu) using a quartz cuvette (1-mm path length).

Results and Discussion

Copolymerization of 1 with 5

The polymerization of monosubstituted acetylene derivatives has been widely investigated using Rh complex catalysts, which enables stereoselective synthesis of the corresponding polyacetylenes of the *cis*-isomers.[16] As

© 2006 WILEY-VCH Verlag GmbH & Co. KGaA, Weinheim